

Journal of Materials Chemistry A

Accepted Manuscript



This is an *Accepted Manuscript*, which has been through the Royal Society of Chemistry peer review process and has been accepted for publication.

Accepted Manuscripts are published online shortly after acceptance, before technical editing, formatting and proof reading. Using this free service, authors can make their results available to the community, in citable form, before we publish the edited article. We will replace this *Accepted Manuscript* with the edited and formatted *Advance Article* as soon as it is available.

You can find more information about *Accepted Manuscripts* in the [Information for Authors](#).

Please note that technical editing may introduce minor changes to the text and/or graphics, which may alter content. The journal's standard [Terms & Conditions](#) and the [Ethical guidelines](#) still apply. In no event shall the Royal Society of Chemistry be held responsible for any errors or omissions in this *Accepted Manuscript* or any consequences arising from the use of any information it contains.

Improvement of the humidity stability of organic/inorganic perovskite solar cells using ultrathin Al₂O₃ layers prepared by atomic layer deposition

Xu Dong^a, Xiang Fang^a, Minghang Lv^a, Bencai Lin^{a,b,c}, Shuai zhang^{a,b,c}, Jianning Ding^{*a,b,c},

Ningyi Yuan^{*a,b,c}

^aCenter for Low-Dimensional Materials, Micro-Nano Devices and Systems, Changzhou University, Changzhou, 213164, Jiangsu, China

^bJiangsu Collaborative Innovation Center of Photovoltaic Science and Engineering, Changzhou University, Changzhou, 213164, Jiangsu, China

^cJiangsu State Key Laboratory for Photovoltaic Engineering and Science, Changzhou University, Changzhou, 213164, Jiangsu, China

* To whom correspondence should be addressed. E-mail: nyuyan@cczu.edu.cn; dingjn@cczu.edu.cn; or ademwy@126.com

Abstract

For successful commercialization of organic/inorganic halide perovskite solar cells, it is necessary to ensure their stability in addition to high efficiency. In this study, the degradation mechanism of organic/inorganic halide structures in humidity was investigated computationally. Owing to the high polarity of water molecules, the unprotected organic/inorganic structure will inevitably decompose in a humidity environment. To improve the ambient stability of the organic/inorganic perovskite solar cells, we introduced an interface modification method using ultrathin compact aluminum oxide (Al₂O₃) layers deposited by atomic layer deposition (ALD). The experiment results showed the ambient stability of the organic/inorganic perovskite solar cell with an ultrathin compact Al₂O₃ layer was greatly improved without a significant reduction in efficiency.

Keywords: organic/inorganic perovskite solar cell, the humidity stability, ultrathin Al₂O₃ layer, atomic layer deposition

Introduction

Hybrid organic/inorganic halide perovskites have attracted significant attention owing to the very rapid progress in their photovoltaic properties. Thus far, much of the effort has focused on the fabrication of high-performance perovskite solar cells based on $\text{CH}_3\text{NH}_3\text{PbI}_3$. The power conversion efficiency (PCE) has been increased to a certified 17.9%, and most recently to 19.3%.¹ Although device stability of 500 h has been reported in nitrogen gas with encapsulation,² it has also been reported that $\text{CH}_3\text{NH}_3\text{PbI}_3$ films easily degrade into other chemical species in the presence of moisture.³ To realize successful commercialization of organic/inorganic halide perovskite solar cells, it is necessary to achieve stability in addition to high efficiencies. However, until now, studies on the degradation mechanisms of organic/inorganic halide structures have been limited and methods to improve the stability are not well understood.

Organic/inorganic perovskites are hybrid layered materials, typically with an AMX_3 structure, where A is an organic cation, M is a smaller metal cation, and X is an anion from the halide series. In these organic/inorganic halides, the organic cations are small and are typically restricted to methylammonium, ethylammonium, and formamidinium.^{4,5} The metal cations are typically divalent metal ions, such as Pb^{2+} and Sn^{2+} ,^{6,7} and the halide anions are I^- , Cl^- , and Br^- .^{8,9} In this study, we introduced a theoretical calculation to analyze the interaction between the inorganic and organic units, and to estimate the stability of the organic/inorganic hybrid structure. Based on the calculation, we found that the strength of the hydrogen bonds between the inorganic and organic units had a significant effect on structural stability. The high polarity of water molecule will inevitably cause the decomposition of the unprotected organic/inorganic structure in a humidity environment. To increase the stability of solar cells, a hydrophobic polymer (Poly[2,5-bis(2-decyldodecyl)pyrrolo[3,4-c]pyrrole-1,4(2H,5H)-dione-(E)-1,2-di(2,20-bithiophen-

5-yl) ethene] (PDPPDBTE)) was employed instead of spiro-OMeTAD (2,2',7,7'-tetrakis-(*N,N*-di-*p*-methoxyphenylamine)-9,9'-spirobifluorene) as a hole-transport material (HTM). Although the hydrophobic polymer prevented water permeation into the porous perovskite, the efficiency of the solar cell was just 9.2%, which was much lower than that of devices based on spiro-OMeTAD.¹⁰ Solution deposition of Al₂O₃ on perovskite improved the stability of perovskite to a certain extent, but the efficiency of this solar cell was only 4.6%.¹¹ Remarkably, a device with no HTM and a 10 μm thick carbon layer as the electrode remained stable for more than 1000 h in ambient air under full sunlight.¹² This stability is the result of the excellent waterproof performance of the carbon layer; however, the efficiency of this device cannot contend with those of devices with an HTM.¹ Here, we report another effective method to retard degradation of the perovskite structure based on an interface modification method that uses ultrathin compact aluminum oxide (Al₂O₃) layers deposited by ALD, which has almost no negative effect on device performance. The self-terminating process in ALD enables angstrom-scale control over the coating thicknesses. The deposited layer's thickness is precisely controllable based on the number of ALD cycles. But also ALD conformally coats high surface area materials. ALD allowed variation of thicknesses at atomic resolution also deep in nanoporous structures, which makes it a superior method as compared to sol-gel techniques.¹³⁻¹⁸ All of these benefits make ALD suitable for depositing ultrathin layers. And ALD techniques can produce continuous, angstrom-level-controlled, pinhole-free oxide films^{19,20} and has been widely used in the production of various types of solar cells.^{21,22} For us, ALD-Al₂O₃ films have been reported to provide effective permeation barriers against oxygen²³ and moisture.^{24,25} We have investigated the influence of ultrathin ALD-Al₂O₃ layers on the performance of organic/inorganic halide

perovskite solar cells.

Computation method

All the calculations were performed using the GAUSSIAN-03 program. The minimum-energy structures of all molecular isomers were completely optimized using density-functional theory (DFT) employing Becke's three-parameter exchange potential and the Lee-Yang-Parr correlation functional (B3LYP). The LanL2DZ basis set was used for metal and halogen atoms, whereas the 6-311++G(d,p) basis set was used for C, N, O, and H atoms. Vibrational mode analyses were systematically carried out to confirm that on a potential energy surface all the optimized geometries corresponded to a local minimum that had no imaginary frequency mode. The structural changes of the molecules under the influence of foreign water molecules were examined. To further investigate the strength of the interaction between the organic-inorganic hybrid and water molecules, a natural bonding orbital (NBO) analysis was carried out. The interaction energies were corrected for the basis set superposition error (BSSE) using the counterpoise correction method of Boys and Bernardi.²⁶

Experimental section

Preparation and stability characterization of $\text{CH}_3\text{NH}_3\text{PbI}_3$

The $\text{CH}_3\text{NH}_3\text{PbI}_3$ layers were prepared in a N_2 -purged glove box using a $\text{CH}_3\text{NH}_3\text{PbI}_3$ precursor solution containing 40 wt% of synthesized $\text{CH}_3\text{NH}_3\text{I}$ powder and PbI_2 in γ -butyrolactone: dimethyl sulfoxide (7:3). This solution was spin-coated onto the compact TiO_2 layers by two consecutive spin-coating steps at 1000 and 5000 rpm for 90 and 30 s, respectively. During the second spin-coating step, toluene (1 mL) was introduced dropwise onto the substrate. The substrate was then dried on a hot plate at 100 °C for 10 min. To investigate the influence of

modifying the $\text{CH}_3\text{NH}_3\text{PbI}_3$ interface with ALD- Al_2O_3 , ultrathin Al_2O_3 films were deposited either beneath or above the spiro-OMeTAD layer on $\text{CH}_3\text{NH}_3\text{PbI}_3$. Because of the humidity sensitivity of $\text{CH}_3\text{NH}_3\text{PbI}_3$, trimethylaluminum (TMA, $\text{Al}_3(\text{CH}_3)_3$) and ozone were chosen as the aluminum and oxygen sources, respectively, to deposit Al_2O_3 layers using the ALD method. High purity nitrogen gas was used as both the carrier and purge gases. In each ALD cycle, TMA was dosed into the reactor for 100 ms, which was then purged for 2 s before and after O_3 was dosed into the reactor for 200 ms. In this study, the deposition temperature was 70 °C, which is lower than the commonly used temperature of 200 °C. This lower temperature was chosen because of the relatively low thermal stability of $\text{CH}_3\text{NH}_3\text{PbI}_3$ and spiro-OMeTAD, and the strong oxidation characteristics of O_3 . The deposition rate was 0.1 nm/cycle. The crystal structures of the films were determined by X-ray diffraction (XRD) analysis with Cu $K\alpha$ radiation (D/max 2500 PC, Rigaku Corporation, Japan; $2\theta/\theta$, $\lambda = 0.1542$ nm) at 40 kV.

Fabrication and characterization of solar cells

Usually, devices are constructed from the bottom (the side from which the light is incident) on fluorine-doped tin oxide (FTO)-coated glass that is coated with a compact layer of n-type TiO_2 , which acts as the electron selective contact. The perovskite layer is then deposited on the n-type compact layer, followed by the p-type hole-conductor, which ensures the collection of holes selectively at the silver cathode. To investigate the influence of ALD- Al_2O_3 interface modification on the performance of the organic/inorganic hybrid solar cells, three different solar cells were fabricated:

$\text{FTO}/\text{TiO}_2/\text{CH}_3\text{NH}_3\text{PbI}_3/\text{spiro-OMeTAD}/\text{Ag}$,

$\text{FTO}/\text{TiO}_2/\text{CH}_3\text{NH}_3\text{PbI}_3/\text{Al}_2\text{O}_3/\text{spiro-OMeTAD}/\text{Ag}$, and $\text{FTO}/\text{TiO}_2/\text{CH}_3\text{NH}_3\text{PbI}_3/\text{spiro-OMeTAD}/\text{Al}_2\text{O}_3/\text{Ag}$.

The 30 nm thick TiO_2 layers were deposited using a sol-gel method with titanium acid

isopropyl ester. The back contact, consisting of a 120 nm thick silver layer, was thermally evaporated.

The photovoltaic characteristics were measured under 100 mW/cm^2 (AM 1.5) illumination using a Keithley 2400 source meter. A solar simulator (500 W Xe lamp) (Japan SAN-EI ELECTRIC XES-40S1) was employed as the light source and the incident light intensity was calibrated by simultaneously using a standard silicon solar cell and a light intensity meter (Radiometer FZ-A). All measurements were performed in air at room temperature with a humidity of 45–50%. Electrochemical impedance spectra (EIS) were conducted using a Zahner IM6ex electrochemical workstation in the dark with a bias of 0.9 V. A perturbation of 10 mV was applied, and the frequency was from 1 MHz to 1 Hz.

Results and Discussion

The precursor solution of $\text{CH}_3\text{NH}_3\text{PbI}_3$ is generally prepared by mixing the powders of $\text{CH}_3\text{NH}_3\text{I}$ and PbI_2 . We first investigated the most stable configurations of $\text{CH}_3\text{NH}_3\text{I}$ and $\text{CH}_3\text{NH}_3\text{PbI}_3$, as shown in Fig. 1a and b, respectively. When CH_3NH_2 and HI solutions are mixed for a long time, $\text{CH}_3\text{NH}_3\text{I}$ can be formed. The calculations suggest that in $\text{CH}_3\text{NH}_3\text{I}$, three hydrogen atoms are covalently bond to the nitrogen atom, and the other three hydrogen atoms are covalently bond to the carbon atom to form the CH_3NH_3^+ cation, which the iodine atom interacts with through hydrogen bonding rather than covalent bonding. To form $\text{CH}_3\text{NH}_3\text{PbI}_3$, usually $\text{CH}_3\text{NH}_3\text{I}$ and PbI_2 are mixed. As shown in Fig. 1b, the Pb atom forms ionic bonds with the three I atoms to form the inorganic PbI_3^- anion, which is bound to the organic $(\text{CH}_3\text{NH}_3)^+$ cation through hydrogen bonds. The binding energy for the formation of $\text{CH}_3\text{NH}_3\text{PbI}_3$ from $\text{CH}_3\text{NH}_3\text{I}$ and PbI_2 is 1.40 eV.

To investigate the interactions between the organic and inorganic molecules, an NBO analysis was carried out. In the NBO analysis, the stabilization energy $E(2)$ for each donor NBO (i) and acceptor NBO (j) associated with delocalization ("2e-stabilization") $i \rightarrow j$ is estimated as:

$$E(2) = \Delta E_{ij} = q_i \frac{F(i,j)^2}{\varepsilon_i - \varepsilon_j}$$

where q_i is the occupancy of the donor orbital, ε_i and ε_j are diagonal elements (orbital energies), and $F(i,j)$ is the off-diagonal NBO Fock matrix element. Vicinal interactions between the delocalizing acceptor orbital and the orbital of the adjacent bonded atom (donor-acceptor NBOs separated by one connecting bond) can influence the molecular properties through delocalization interactions, known as the hyper conjugative effect. Table 1 lists the stabilization energies (in kcal/mol) of the main interactions between the organic unit, inorganic unit, and H₂O in the CH₃NH₃PbI₃ system with and without H₂O. As shown in Table 1, in CH₃NH₃PbI₃, there are two major types of vicinal interactions; namely, (1) $n(I) \rightarrow \sigma_{H-N}^*$ (the lone pair of an I atom and the antibonding orbital of an (H–N) bond) and (2) $n(I) \rightarrow \sigma_{H-C}^*$ (the lone pair of an I atom and the antibonding orbital of an (H–C) bond). The stabilization energies of the two stereoelectronic interactions (1) are about 19 kcal/mol, and are much larger than that of interaction (2). To investigate the influence of humidity on the stability of CH₃NH₃PbI₃, we calculated systems composed of CH₃NH₃PbI₃ and water molecules; the most stable systems are shown in Fig. 1c and 1d. The energy of the CH₃NH₃PbI₃•H₂O system is 0.526 eV lower than the total energy of the free CH₃NH₃PbI₃ and H₂O molecules, which means it is very easy for water to be adsorbed onto CH₃NH₃PbI₃. When a CH₃NH₃PbI₃ molecule encounters one water molecule, the weak donor-acceptor interaction (2) in the CH₃NH₃PbI₃ molecule is broken and the two stereoelectronic interactions (1) are weakened; namely, the stabilization energies decrease from ~19 to ~13

kcal/mol. Meanwhile, two further interactions between $\text{CH}_3\text{NH}_3\text{PbI}_3$ and H_2O molecules are established: (3) $n(\text{I}) \rightarrow \sigma_{\text{O-H}}^*$ and (4) $n(\text{O}) \rightarrow \sigma_{\text{N-H}}^*$. The stabilization energy of the donor-acceptor interaction (4) between the lone pair of the O atom in H_2O and the antibonding orbital of an (N–H) bond in the organic CH_3NH_3 unit is 21.8 kcal/mol, which is considerable larger than that between the PbI_3 and CH_3NH_3 units. As a result, one water molecule will reduce the stability of $\text{CH}_3\text{NH}_3\text{PbI}_3$. Although water weakens the interactions between the PbI_3 and CH_3NH_3 units in $\text{CH}_3\text{NH}_3\text{PbI}_3$, the structure of $\text{CH}_3\text{NH}_3\text{PbI}_3$ is not completely destroyed. However, when a $\text{CH}_3\text{NH}_3\text{PbI}_3$ molecule encounters two water molecules, as shown in Table 1, the hydrogen bonds between the PbI_3 and CH_3NH_3 units are nearly broken. The interaction (4) between the CH_3NH_3 unit and H_2O is much larger than that between the PbI_3 and CH_3NH_3 units in $\text{CH}_3\text{NH}_3\text{PbI}_3$, which induces complete decomposition of $\text{CH}_3\text{NH}_3\text{PbI}_3$. The results of this calculation are in agreement with experimental observations,¹ where in low humidity $\text{CH}_3\text{NH}_3\text{PbI}_3$ is not easily decomposed and remains relatively stable, but once the humidity is increased the structure is quickly destroyed.

It is clear from the above calculation results that hydrogen bonding between the inorganic PbI_3 unit and organic CH_3NH_3 unit plays a decisive role in the stability of $\text{CH}_3\text{NH}_3\text{PbI}_3$. Therefore, two possible approaches to improve the stability of $\text{CH}_3\text{NH}_3\text{PbI}_3$ are suggested. The first is to replace I atoms with more electronegative Br and Cl atoms. The second is to replace the CH_3NH_3 unit with an organic group that is more polar. For this reason, we calculated the most stable structures of $\text{CH}_3\text{NH}_3\text{PbI}_2\text{Br}$, $\text{CH}_3\text{NH}_3\text{PbIBr}_2$, $\text{CH}_3\text{NH}_3\text{PbI}_2\text{Cl}$, and $\text{CH}_3\text{NH}_3\text{PbICl}_2$. The structures of $\text{CH}_3\text{NH}_3\text{PbI}_2\text{Cl}$ and $\text{CH}_3\text{NH}_3\text{PbICl}_2$ are similar to those of $\text{CH}_3\text{NH}_3\text{PbI}_2\text{Br}$ and $\text{CH}_3\text{NH}_3\text{PbIBr}_2$, which are presented in Fig. 1e and 1f. As shown in Table 1, the stabilization energy of the vicinal interactions (1) between the organic and inorganic units in the hybrid molecule increases, which

means the substitution of Br or Cl for I does somewhat improve the stability of the organic/inorganic molecule. The donor-acceptor interactions between $\text{CH}_3\text{NH}_3\text{PbI}_2\text{Br}$, $\text{CH}_3\text{NH}_3\text{PbIBr}_2$, $\text{CH}_3\text{NH}_3\text{PbI}_2\text{Cl}$, or $\text{CH}_3\text{NH}_3\text{PbICl}_2$ and water molecules are also tabulated. Because H_2O is highly polar, similar to $\text{CH}_3\text{NH}_3\text{PbI}_3$, when the organic CH_3NH_3 unit in $\text{CH}_3\text{NH}_3\text{PbI}_2\text{Br}$, $\text{CH}_3\text{NH}_3\text{PbIBr}_2$, $\text{CH}_3\text{NH}_3\text{PbI}_2\text{Cl}$, and $\text{CH}_3\text{NH}_3\text{PbICl}_2$ encounters H_2O , bonds to two H_2O molecules will be formed and the organic/inorganic structure will be destroyed. Although the stabilities of $\text{CH}_3\text{NH}_3\text{PbI}_2\text{Br}$, $\text{CH}_3\text{NH}_3\text{PbIBr}_2$, $\text{CH}_3\text{NH}_3\text{PbI}_2\text{Cl}$ and $\text{CH}_3\text{NH}_3\text{PbICl}_2$ are somewhat improved compared with $\text{CH}_3\text{NH}_3\text{PbI}_3$, the effect is not great enough to inhibit degradation by H_2O , which is in agreement with the report on the improvement of the stability of $\text{MAPb}(\text{I}_{1-x}\text{Br}_x)_3$ when the content of Br was controlled.⁸

In addition, we chose the organic molecules $\text{NH}_2\text{CH}_2\text{NH}_2$ and $\text{NH}_2\text{CH}_2\text{CH}_2\text{NH}_2$ to replace CH_3NH_2 in the organic/inorganic hybrid molecules. Fig. 2 shows the most stable configurations of these molecules and the systems with two water molecules. The donor-acceptor interactions between $\text{NH}_2\text{CH}_2\text{NH}_3\text{PbI}_3$ or $\text{NH}_2\text{CH}_2\text{CH}_2\text{NH}_3\text{PbI}_3$ and water molecules were also calculated, as listed in Table 2. As shown in Table 2, in structures 2a and 2c the stabilization energy for the interaction between the lone pair of I and the antibonding orbital of (N-H) is smaller. The large $n(\text{I}) \rightarrow \sigma^*(\text{N-H})$ stabilization energy determined for $\text{NH}_2\text{CH}_2\text{NH}_3\text{PbI}_3$ suggested that, compared with $\text{CH}_3\text{NH}_3\text{PbI}_3$ and $\text{NH}_2\text{CH}_2\text{CH}_2\text{NH}_3\text{PbI}_3$, this molecule is relatively more stable. Overall, the calculations suggest that because of the large polarity of water, the organic/inorganic structure will inevitably change in a humidity environment. Therefore, packaging and protecting the organic/inorganic perovskite will be a prerequisite for stability.

To retard degradation of the perovskite structure in a humidity environment, we chose the

ALD method to deposit ultrathin Al_2O_3 films on $\text{CH}_3\text{NH}_3\text{PbI}_3$. Meanwhile, we fabricated a series of perovskite solar cells with the FTO/ TiO_2 /perovskite/ Al_2O_3 /spiro-OMeTAD/Ag structure. Fig. 3a shows the X-ray diffraction patterns of $\text{CH}_3\text{NH}_3\text{PbI}_3$ covered with Al_2O_3 layers deposited using 1, 2, or 3 ALD cycles. The main diffraction peaks at 14.12° , 28.44° , and 43.23° are assigned to the 110, 220, and 330 peaks of $\text{CH}_3\text{NH}_3\text{PbI}_3$, respectively, with an orthorhombic crystal structure. Notably, there is the signature of a peak at 12.65° , which is the (001) diffraction peak of PbI_2 . As the number of deposition cycles increased, this peak became stronger, indicating an increase in the PbI_2 content in the $\text{CH}_3\text{NH}_3\text{PbI}_3$ layer. Although a low deposition temperature of 70°C was chosen, decomposition of $\text{CH}_3\text{NH}_3\text{PbI}_3$ was still not completely avoided because the strong oxidizer O_3 was used. The current-density/voltage (J - V) curves measured in an air environment for the solar cells with different deposition cycles of Al_2O_3 layers on the perovskite layer are shown in Fig. 3b. Devices fabricated without an Al_2O_3 layer produced a short-circuit photocurrent (J_{sc}) of 20.35 mA cm^{-2} and an open-circuit voltage (V_{oc}) of 1.05 V, which with a fill factor (FF) of 0.71 yielded an efficiency of 15.2%. With the deposition of Al_2O_3 layers on the perovskite layers, the values of J_{sc} , V_{oc} , and FF all decreased. We speculated that the presence of PbI_2 , resulting from the decomposition of $\text{CH}_3\text{NH}_3\text{PbI}_3$ during the ALD deposition process, decreased the performance of the solar cells. Therefore, we modified the solar cell structure as FTO/ TiO_2 / $\text{CH}_3\text{NH}_3\text{PbI}_3$ /spiro-OMeTAD/ Al_2O_3 /Ag, with the Al_2O_3 layers prepared on top of the spiro-OMeTAD layers. Fig. 3c shows a comparison of the XRD patterns of $\text{CH}_3\text{NH}_3\text{PbI}_3$ that has been covered with a 100 nm spiro-OMeTAD layer and subsequently with different cycles of Al_2O_3 layers. A close examination of the region around the (110) diffraction peak at 14.12° shows no measurable peak at 12.65° for PbI_2 , indicating a high level of phase purity, even when five cycles

of Al₂O₃ layers were deposited. The $J-V$ curves for these solar cells (Fig. 3d) indicated that the deposition of 1–3 cycles of Al₂O₃ layers had no obvious effect on the performance of solar cell, but when the number of cycles was increased to five, the current decreased sharply. The Al₂O₃ layers act as protection against air, and can reduce the permeability toward moisture, thus enhancing the stability of the solar cells. However, if the film is too thick, a significant reduction in the quantum tunneling of the holes is expected, and the charge would therefore not be collected. Thick Al₂O₃ layers, which increase the series resistance of the solar cell, would also be responsible for the lower fill factor and open-circuit voltage. To further understand the influence of the ALD-Al₂O₃ on the devices, EIS measurements for each the perovskite solar cells with or without Al₂O₃ were carried out. In our case, since ultrathin ALD-Al₂O₃ acted as waterproofer between HTM and contact electrode (CE), we mainly concerned the RC elements at HTM/CE interfaces. Nyquist plots of the devices are shown in Fig.5. It has been reported that in the EIS spectra of perovskite solar cells, the semicircle in the high frequency range is attributed to the diffusion of holes through the HTM which is modeled by a HTM resistance, R_{HTM} .²⁷⁻³⁰ The series resistance (R_s) is equal to the value of high-frequency intercept on the real axis. The right incomplete semicircle in the low frequency range is a transmission line, which is mainly attributed to recombination resistance (R_{rec}) between the perovskite film and the TiO₂ film. It can be seen from Nyquist plots in the figure that the R_s and R_{HTM} values of the perovskite solar cell with 3-cycle-ALD-Al₂O₃ on HTM are a little larger than those of that without ALD-Al₂O₃. However, the perovskite solar cell with 5-cycle-ALD-Al₂O₃ has a much higher R_s and R_{HTM} . The EIS analyses are consistent with the $I-V$ measurements of the perovskite solar cells.

XRD measurements were also performed to explore film stability and degree of degradation

over time. Fig. 4 shows a comparison of the XRD spectra of perovskite films with and without ultrathin ALD- Al_2O_3 layers on the HTM that were stored in 50% humidity for 0–24 days. In the perovskite film without spiro-OMeTAD and Al_2O_3 layers, most of the perovskite peaks disappeared after 5 days and an increased signal from PbI_2 was observed. In addition, the color of this film changed from dark brown to yellow because of perovskite decomposition. The perovskite film with a 100 nm thick spiro-OMeTAD layer showed XRD peaks corresponding to both crystalline perovskite and PbI_2 . As the number of storage days increased, the PbI_2 content in the film increased (Fig. 4a). Notably, in the perovskite film with a 100-nm-spiro-OMeTAD layer and 3-cycle ALD- Al_2O_3 layers, the main perovskite XRD peaks remained unchanged without the formation of any new peaks, even after being exposed to air for 24 days (Fig. 4c). Based on these results, we characterized the air stability of unencapsulated perovskite solar cells as a function of storage time in air at room temperature, as shown in Fig.4b and Fig.4d. With 3-cycle ALD- Al_2O_3 layers deposited on the spiro-OMeTAD layer, the solar cells exhibited significantly improved stability compared with that for the solar cell without ALD- Al_2O_3 . The PCE of 12.9% was ~90% of the initial value, even after storage for 24 days in air (Fig.6).

Conclusion

We used molecular structure modeling to explain the degradation mechanisms of organic/inorganic hybrid structures and found that the hydrogen bonding interactions between the inorganic PbI_3 unit and organic CH_3NH_3 unit play an important role in determining the stability of $\text{CH}_3\text{NH}_3\text{PbI}_3$. The calculations suggested that the organic/inorganic structure would inevitably change in a humidity environment because of the high polarity of water. Therefore, to inhibit degradation of the perovskite solar cells in a humidity environment, the organic/inorganic

perovskite must be protected. We used the ALD method to deposit ultrathin Al_2O_3 films on the HTM layer. Ultrathin ALD- Al_2O_3 acted as a waterproofer and isolated the $\text{CH}_3\text{NH}_3\text{PbI}_3$ layers from moisture, thus realizing enhanced stability of the device, and as far as possible do not affect performance by the tunneling effect. Remarkably, the PCE of the solar cell with ALD- Al_2O_3 retained ~90% of its initial value after 24 days storage in air. The concept and method of this effective solution to improve the stability of these devices can be applied to commercialize perovskite solar cell products.

Acknowledgements

This work was supported by the National Natural Science Foundation of china (Grant No. 51272033), the Priority Academic Program Development of Jiangsu Higher Education Institutions, the Natural Science Foundation of the Jiangsu Higher Education Institutions of China (Grant No. 14KJA430001, EEKJA48000).

Figure Legends:

Fig.1 The most stable configurations of (a) $\text{CH}_3\text{NH}_3\text{I}$; (b) $\text{CH}_3\text{NH}_3\text{PbI}_3$; (c) $\text{CH}_3\text{NH}_3\text{PbI}_3 \bullet \text{H}_2\text{O}$; (d) $\text{CH}_3\text{NH}_3\text{PbI}_3 \bullet 2\text{H}_2\text{O}$; (e) $\text{CH}_3\text{NH}_3\text{PbI}_2\text{Br}$; (f) $\text{CH}_3\text{NH}_3\text{PbIBr}_2$; (g) $\text{CH}_3\text{NH}_3\text{PbI}_2\text{Br} \bullet 2\text{H}_2\text{O}$; (h) $\text{CH}_3\text{NH}_3\text{PbIBr}_2 \bullet 2\text{H}_2\text{O}$

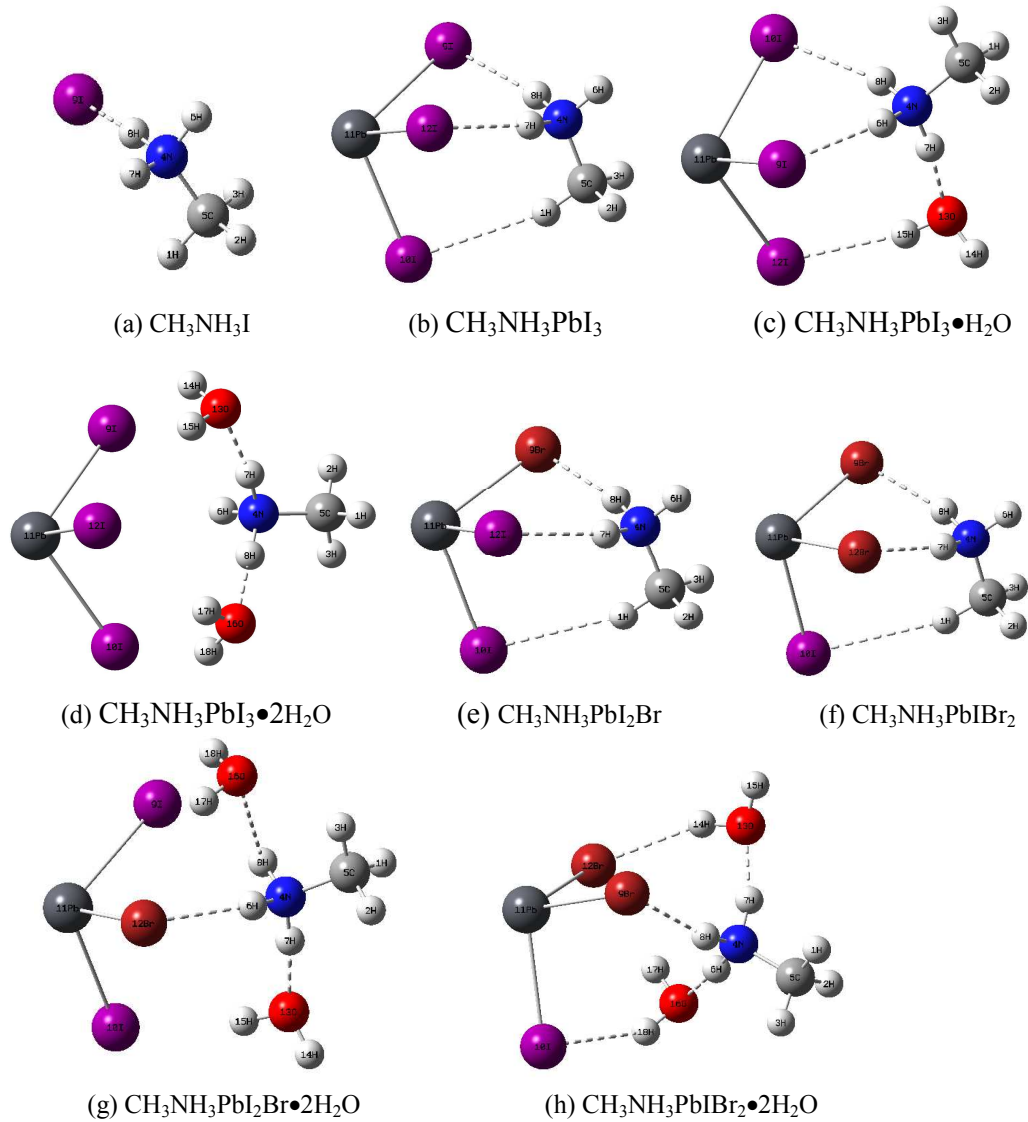
Fig.2 The most stable configurations of (a) $\text{NH}_2\text{CH}_2\text{NH}_3\text{PbI}_3$; (b) $\text{NH}_2\text{CH}_2\text{NH}_3\text{PbI}_3 \bullet 2\text{H}_2\text{O}$; (c) $\text{NH}_2\text{CH}_2\text{CH}_2\text{NH}_3\text{PbI}_3$; (d) $\text{NH}_2\text{CH}_2\text{CH}_2\text{NH}_3\text{PbI}_3 \bullet 2\text{H}_2\text{O}$

Fig.3 (a) XRD of the perovskite layers with ALD- Al_2O_3 with different cycles; (b) J-V characteristics for $\text{FTO}/\text{bl-TiO}_2/\text{CH}_3\text{NH}_3\text{PbI}_3/\text{Al}_2\text{O}_3/\text{HTM}/\text{Ag}$, where the Al_2O_3 are fabricated with different cycles; (c) XRD of the perovskite layers with 100nm-HTM and different cycles ALD- Al_2O_3 ; (d) J-V characteristics for $\text{FTO}/\text{bl-TiO}_2/\text{CH}_3\text{NH}_3\text{PbI}_3/\text{HTM}/\text{Al}_2\text{O}_3/\text{Ag}$, where the Al_2O_3 are fabricated with different cycles;

Fig.4 (a) XRD of the perovskite layers with 100nm-HTM placing at room temperature in the humidity of 50% with varying duration (as indicated); (b) J-V characteristics for $\text{FTO}/\text{bl-TiO}_2/\text{CH}_3\text{NH}_3\text{PbI}_3/\text{HTM}/\text{Ag}$ with placing at room temperature in the humidity of 50% with 0 and 24 days; (c) XRD of the perovskite layers with 100nm-HTM and 3-cycle ALD- Al_2O_3 placing at room temperature in the humidity of 50% with varying duration (as indicated); (d) J-V characteristics for $\text{FTO}/\text{bl-TiO}_2/\text{CH}_3\text{NH}_3\text{PbI}_3/\text{HTM}/\text{Al}_2\text{O}_3/\text{Ag}$ with placing at room temperature in the humidity of 50% with 0 and 24 days;

Fig.5 Nyquist plots of solar cells with 0-cycle-ALD- Al_2O_3 , 3-cycle-ALD- Al_2O_3 , 5-cycle-ALD- Al_2O_3 on HTM, and the equivalent circuit employed to fit the spectra.

Fig.6 The histogram of the PCE of thirty solar cells after 24 days in air compared with the original efficiency

**Fig.1**

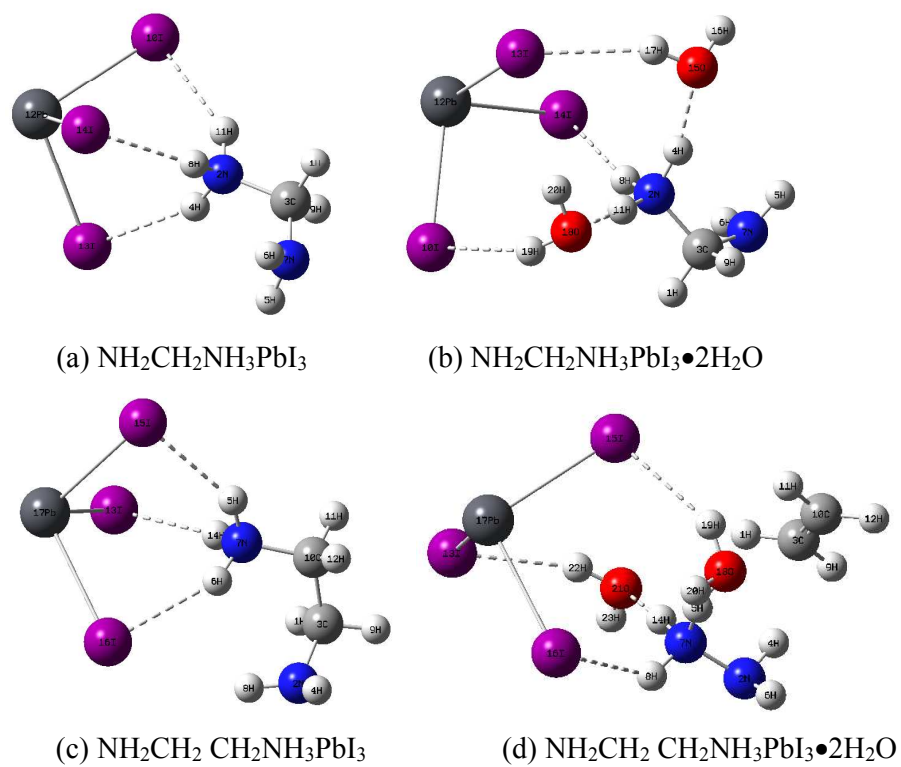


Fig.2

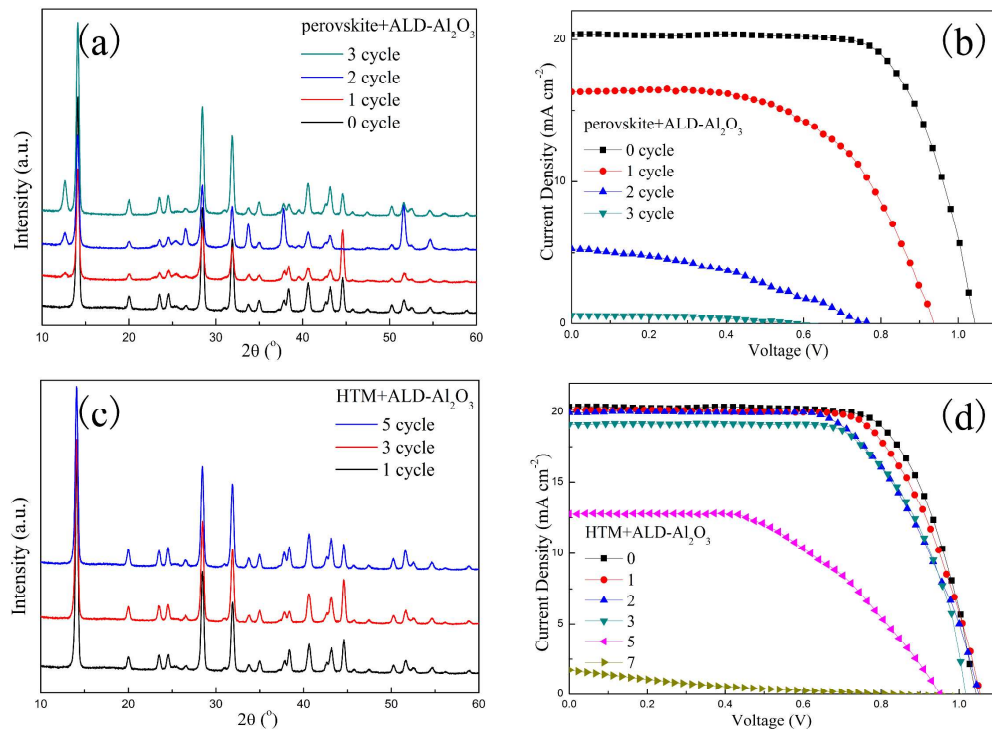


Fig.3

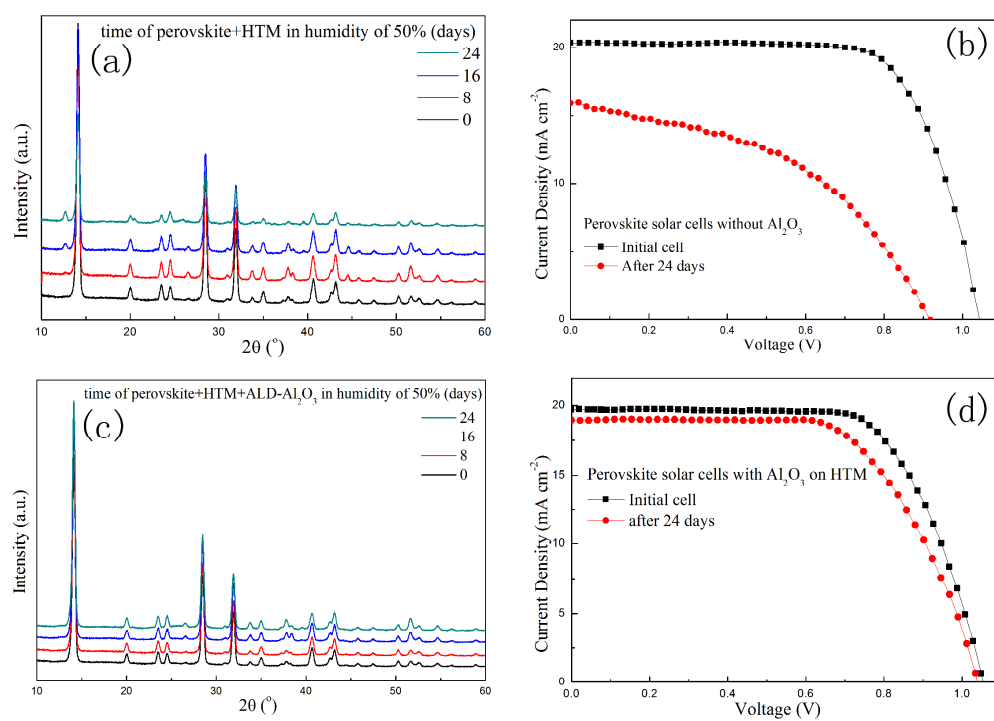


Fig.4

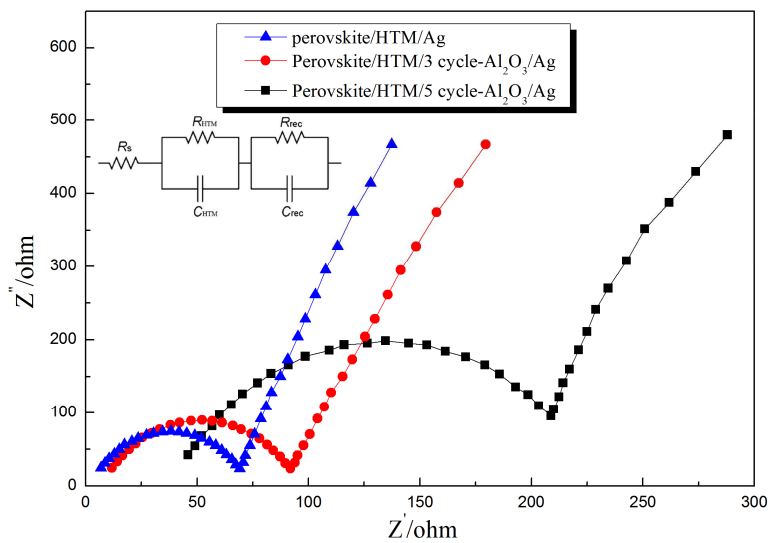


Fig.5

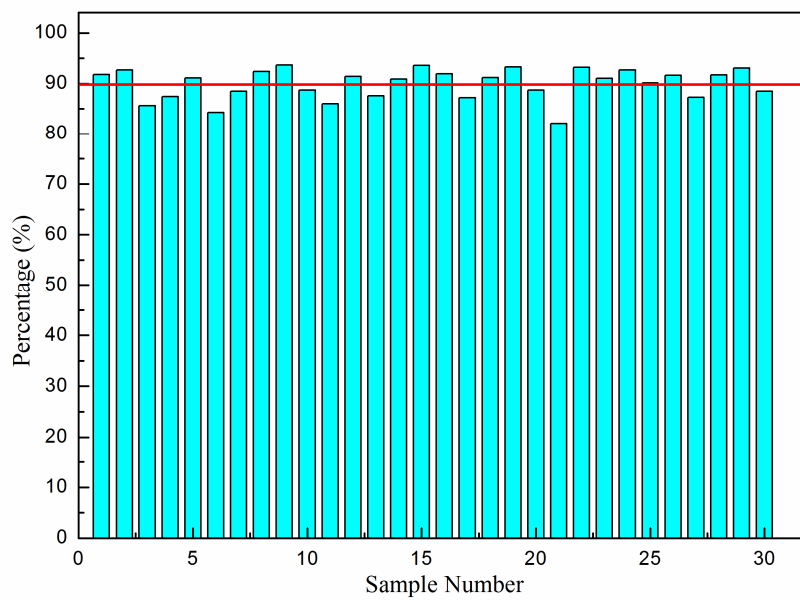
**Fig.6**

Table 1 Stabilization energy (in Kcal/mol) of main interactions between organic unit, inorganic unit or H₂O molecule in the systems of CH₃NH₃PbI₃, CH₃NH₃PbI₂Br, CH₃NH₃PbI₂Cl, CH₃NH₃PbI₂Br₂, CH₃NH₃PbI₂Cl, CH₃NH₃PbICl₂ with and without H₂O (X represent halogen elements)

structure		CH ₃ NH ₃ PbI ₃	CH ₃ NH ₃ PbI ₂ Br	CH ₃ NH ₃ PbI ₂ Br ₂	H ₃ NH ₃ PbI ₂ Cl	H ₃ NH ₃ PbICl ₂
	Donor-Accept	Stabilization energy				
	n(X)→σ*(N-H)	18.59(I)	21.98(Br)	20.63(Br)	26.64(Cl)	22.52(Cl)
	n(X)→σ*(N-H)	18.70(I)	17.08(I)	20.63(Br)	15.26(I)	22.52(Cl)
	n(X)→σ*(H-C)	2.19(I)	1.04(I)	1.98(I)	1.97(I)	1.84(I)
H ₂ O	n(X)→σ*(N-H)	13.86(I)	16.30(Br)	14.90(Br)	19.30(Cl)	16.57(Cl)
	n(X)→σ*(N-H)	12.98(I)	12.34(I)	14.61(Br)	11.24(I)	16.43(Cl)
	n(X)→σ*(O-H)	6.71(I)	6.73(I)	7.24(I)	6.91(I)	6.33(I)
	n(O)→σ*(N-H)	21.89	21.29	21.14	20.35	19.38
2H ₂ O	n(X)→σ*(N-H)	2.97(I)	5.64(Br)	14.09(Br)	6.35(Cl)	16.41(Cl)
	n(X)→σ*(O-H)	2.98(I)	3.45(I)	5.22(Br)	3.12(I)	5.66(I)
	n(X)→σ*(O-H)	1.90(I)	1.52(I)	3.44(I)	2.64(I)	3.14(I)
	n(O)→σ*(N-H)	22.47	25.32	24.83	25.37	25.20
	n(O)→σ*(N-H)	25.81	21.09	17.67	20.45	16.95

(X represent halogen elements)

Table 2 Stabilization energy (in Kcal/mol) of main interactions between organic unit, inorganic unit or H₂O molecule in the systems of CH₃NH₃PbI₃, NH₂CH₂NH₃PbI₃ and NH₂CH₂CH₂NH₃PbI₃

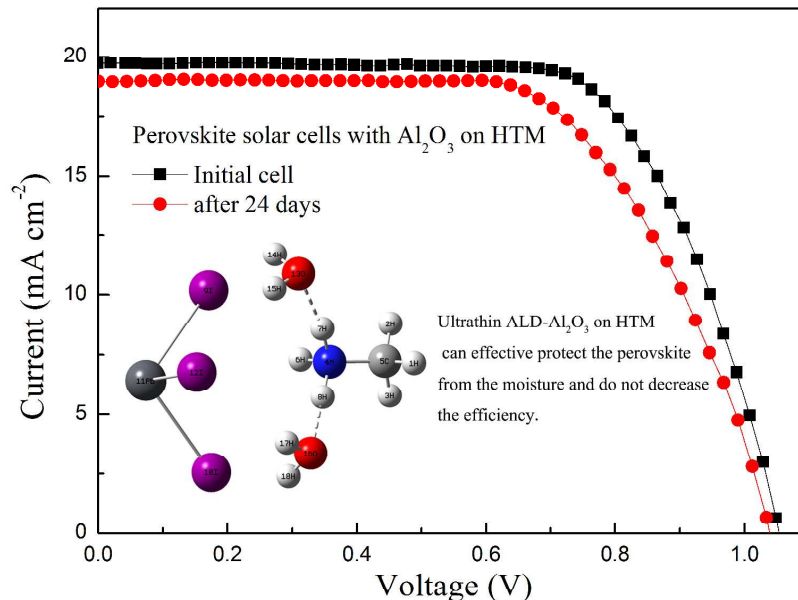
	Without H ₂ O		2H ₂ O	
	Donor-Accept	Stabilization energy	Donor-Accept	Stabilization energy
CH ₃ NH ₃ PbI ₃	n(I19)→σ*(N4-H8)	18.59	n(I9)→σ*(N4-H6)	2.97
	n(I11)→σ*(N4-H7)	18.70	n(I10)→σ*(O16-H18)	2.98
	n(I10)→σ*(H1-C5)	2.19	n(I12)→σ*(O13-H15)	1.90
			n(O13)→σ*(N4-H7)	22.70
			n(O16)→σ*(N4-H8)	25.81
NH ₂ CH ₂ NH ₃ PbI ₃	n(I14)→σ*(N2-H8)	12.81	n(I14)→σ*(N2-H8)	11.11
	n(I13)→σ*(N2-H4)	12.85	n(I13)→σ*(O15-H17)	4.23
	n(I10)→σ*(N2-N11)	5.03	n(I10)→σ*(O18-H19)	4.02
			n(O15)→σ*(N2-H4)	16.24
			n(O18)→σ*(N2-H11)	25.23
NH ₂ CH ₂ CH ₂ NH ₃ PbI ₃	n(I15)→σ*(N7-H5)	8.70	n(I16)→σ*(N7-H8)	2.65
	n(I16)→σ*(N7-H6)	10.82	n(I15)→σ*(O18-H19)	4.32
	n(I13)→σ*(N7-H14)	12.69	n(I13)→σ*(O21-H22)	6.91
			n(O18)→σ*(N7-H5)	23.90
			n(O21)→σ*(N7-H14)	25.40

References

1. H. Zhou, Q. Chen, G. Li, S. Luo, T. B. Song, H. S. Duan, Z. Hong, J. You, Y. Liu, Y. Yang, *Science*, 2014, **345**, 542
2. J. Burschkaet, N. Pellet, S-J Moon, R Humphry-Baker, P Gao, M K. Nazeeruddin and M Graätzel, *Nature*, 2013, **499**, 316.
3. A. Dualeh, N. Te'treault, T. Moehl, P. Gao, M. K. Nazeeruddin and M. Graätzel, *Adv. Funct. Mater.*, 2014, **24**, 3250.
4. N. J. Jeon, H. G. Lee, Y. C. Kim, J. Seo, J. H. Noh, J. Lee and S. Il Seok, *J. Am. Chem. Soc.*, 2014, **136**, 7837.
5. G. E. Eperon, S. D. Stranks, C. Menelaou, M. B. Johnston, L. M. Herz and H. J. Snaith. *Energy Environ. Sci.* 2014, **7**, 982.
6. Z. L. Zhu, J. N. Ma, Z. L. Wang, C. Mu, Z. Fan, L. L. Du, Y. Bai, L. Z. T. Fan, H. Yan, D. L. Phillips and S. H. Yang, *J. Am. Chem. Soc.*, 2014, **136**, 3760.
7. Y. Ogomi, A. Morita, S. Tsukamoto, T. Saitho, N. Fujikawa, Q. Shen, T. Toyoda, K. Yoshino, S. S. Pandey, T. Ma, and S. Hayase, *J. Phys. Chem. Lett.*, 2014, **5**, 1004.
8. J. H. Noh, S. H. Im, J. H. Heo, T. N. Mandal, and S. Il. Seok, *Nano Lett.*, 2013, **13**, 1764.
9. Y. Zhao and K. Zhu, *J. Phys. Chem. C*, 2014, **118**, 9412.
10. Y. S. Kwon, J. Lim, H. J. Yun, Y. H. Kim and T. Park, *Energy Environ. Sci.*, 2014, **7**, 1454.
11. G. Niu, W. Li, F. Meng, L. Wang, H. Dong and Y Qiu, *J. Mater. Chem. A.*, 2014, **2**, 705.
12. A. Y. Mei, X. Li, L. F. Liu, Z. L. Ku, T. F. Liu, Y. G. Rong, M. Xu, M. Hu, J. Z. Chen, Y. Yang, M. Grätze, H. W. Han, *Science.*, 2014, **345**, 295.
13. George, S. M, *Chem.Rev*, 2009, **110**, 111.
14. C. Prasittichai and J. T. Hupp, *J. Phys. Chem. Lett.*, 2010, **1**, 1611.

15. T-C Tien, F-M Pan, L-P Wang, C-H Lee, Y-L Tung, S-Y Tsai, C Lin, F-Y. Tsai and S-J Chen, *Nanotechnology*, 2009, **20**, 305201.
16. L. Wang , J. J. Travis , A. S. Cavanagh , X. H. Liu , S. P. Koenig, P. Y. Huang, S. M. George and J. S. Bunch, *Nano Lett.*, 2012, **12** , 3706.
17. L. J. Antila, M. J. Heikkilä, V. Aumanen, M. Kemell, P. Myllyperkiö, M. Leskelä and J. E. I. Korppi-Tommola, *J. Phys. Chem. Lett.*, 2010, **1**, 536.
18. M. Law , L. E. Greene , A. Radenovic , T. Kuykendall , J. Liphardt and P. Yang , *J. Phys. Chem. B*, 2006, **110** , 22652.
19. D. N. Goldstein, J. A. McCormick and S. M. George, *J. Phys. Chem. C.*, 2008, **112**, 19530.
20. K. Yu, X. Lin, G. H. Lu, Z. H. Wen, C. Yuan and J. C. Chen, *RSC Adv.*, 2012, **2**, 7843.
21. X. Dong, H. W. Hu, B. C. Lin, J. N. Ding and N. Y. Yuan, *Chem. Commun.*, 2014, **50**, 14405.
22. Y. Z. Wu, X. D. Yang, H. Chen, K. Zhang, C. J. Qin, J. Liu, W. Q. Peng, A. Islam, E. B. Bi, F. Ye, M. S. Yin, P. Zhang, L. Y. Han, *Appl. Phys. Express.*, 2014, **7**, 052301
23. S. M. George, *Chem. Rev.*, 2010, **110**, 111.
24. A. I. Abdulagatov, Y. Yan, J. R. Cooper, Y. Zhang, Z. M. Gibbs, A. S. Cavanagh, R. G. Yang, Y. C. Lee and S. M. Georg, *Appl. Mater. Interfaces.*, 2011, **3**, 4593.
25. E. Langereis, M. Creatore, S. B. S. Heil, M. C. M. Van de Sanden, W. M. M. Kessels, *Appl. Phys. Lett.*, 2006, **89**, 8.
26. S.F. Boys, F. Bernardi, *Mol. Phys.*, 1970. **19**. 553.
27. W. J. Ke, G. J. Fang, J. Wang, P. L. Qin, H. Tao, H. W. Lei, Q. Liu, X. Dai and X. Z. Zhao, *ACS Appl. Mater. Interfaces*, 2014, **6**, 15959.
28. P. Qin, S. Tanaka, S. Ito, N. Tetreault, K. Manabe, H. Nishino, M. K. Nazeeruddin and M. Grätzel, *Nature Communications*, 2014, **5**, 3834.
29. Y. G. Rong, Z. L. Ku, A. Y. Mei, T. F. Liu, M. Xu, S. Ko, X. Li and H. W. Han, *J. Phys. Chem. Lett.*, 2014, **5**, 2160.
30. B. J. Kim, D. H. Kim, Y-Y Lee, H-W Shin, G. S. Han, J. S. Hong, K. Mahmood, T. Ahn, Y-C Joo, K. S. Hong, N-G Park, S. Lee, H. S. Jung, *Energy Environ. Sci.*, 2015, DOI:

10.1039/C4EE02441A.



The high polarity of water molecules inevitably cause the decomposition of perovskite, we retard the degradation by introducing an ultrathin ALD- Al_2O_3 layer which has almost no negative effect on performance.